SOIL, 12, 1079–1099, 2026
https://doi.org/10.5194/soil-12-1079-2026
© Author(s) 2026. This work is distributed under
the Creative Commons Attribution 4.0 License.

SOIL Open Access EGU

Microbial carbon use efficiency emerges from interactions between soil structure and life-history strategies

Maëlle Maestrali[1], Naoise Nunan[1], Antsa Sarobidy-Randrianantenaina[1], Haotian Wu[2], Steffen A. Schweizer[2], and Xavier Raynaud[1]

[1]Sorbonne Université, Université Paris Cité, Univ. Paris Est Créteil, CNRS, IRD, INRAE, Institut d'écologie et des sciences de l'environnement de Paris, IEES, 75005 Paris, France
[2]Technical University of Munich, TUM, School of Life Science, Chair of Soil Science, Emil-Ramann Straße 2, 85354 Freising, Germany

Correspondence: Maëlle Maestrali (maelle.maestrali@uni-hohenheim.de)

Received: 31 March 2026 – Discussion started: 10 April 2026
Revised: 11 August 2026 – Accepted: 7 October 2026 – Published: 2 November 2026

Abstract. Microbial carbon use efficiency (CUE) is believed to be a key regulator of the accumulation of persistent soil organic carbon. Microbial processing of organic carbon in soil occurs in the pore network, the properties of which are known to affect microbial activity. However, the effects of interactions between pore architecture and microbial life-history strategies on carbon dynamics, and how these interactions are modulated by moisture conditions, remain poorly understood.

Here, we use a spatially explicit model based on a cellular automaton, applied to realistic soil pore networks derived from X-ray tomographic images, to investigate how pore geometry and organic matter distribution shape microbial dynamics and CUE. The model explicitly represents r- and K-strategists that are either motile or immobile, and have different resource requirements for growth, maintenance and motility. The constraints imposed by the moisture conditions on substrate diffusion and the spatial domain in which motile bacteria can effectively disperse are explicitly represented in the model, in order to capture how moisture regulates decomposer access to resources.

The simulations show that pore architecture has a significant effect on microbial CUE. Micropores promoted high CUE and a dominance of K-strategists by limiting substrate diffusion, reducing pore connectivity, and constraining microbial access to spatially isolated resources. In contrast, macropores with high connectivity and greater substrate accessibility favour r-strategists, rapid biomass turnover and lower CUE. Motility emerges as advantageous in connected, carbon-rich macropores, but energetically unfavourable in confined or poorly connected micropores, where immobile strategies outperform motile ones.

Overall, our results indicate that microbial CUE is not an intrinsic property of life-strategies alone, but emerges from the interaction between microbial life-strategies and pore-scale physical constraints. This study suggests that soil structure influences microbial strategies by limiting resource availability and dispersal.

Published by Copernicus Publications on behalf of the European Geosciences Union.

1 Introduction

Soil structure refers to the three-dimensional spatial arrangement of solid constituents and voids at different scales (Rabot et al., 2018). Soil pore space is directly linked to soil functions because it governs air/water transport and microbial colonization (Kravchenko et al., 2020; Schlüter et al., 2020). which are essential for determining the efficiency of microbial processes and the carbon cycle (Kravchenko and Guber, 2017; Schimel and Schaeffer, 2012). The size and connectivity of soil pores regulate nutrient diffusion and gas exchange, which can profoundly affect the survival and colonization of microenvironments by microorganisms (Kravchenko and Guber, 2017; Schlüter et al., 2022). In soil, microorganisms tend to selectively inhabit soil pores of different sizes (Li et al., 2024). It has been suggested that the properties of the pores in which microbial decomposers are active influence the rates of OM decomposition and, thus, its persistence (Kravchenko and Guber, 2017; Chenu et al., 2025 ; Maestrali et al., 2026). The fate of organic carbon (OC) depends largely on the ability of resident microorganisms to utilize it, as well as on their spatial access to it (Lehmann et al., 2020; Shi et al., 2021). The decomposition of OC depends on the encounter between organic matter (OM) and decomposers or extracellular enzymes. If this encounter is limited by the structural properties of the microbial environment, decomposition cannot take place, regardless of the properties of the OM (Dignac et al., 2017).

While pores with throat diameters $< 1\,\mu m$ are generally inaccessible to microbes, due to size exclusion, pores between 1 and 10 µm can be colonized by microorganisms, depending on their connectivity to the surrounding pore network. Larger pores ($> 10\,\mu m$) offer more space for microbial colonies and fungal hyphae. Previous studies suggest that pore size and connectivity influence the distribution of microbial strategies, with fast-growing copiotrophs often associated with well-connected, resource-rich environments, and slow-growing oligotrophs dominating in more isolated or resource-limited conditions (Li et al., 2024). However, the extent to which interactions among the physical structure of the pore network, the spatial distribution of resources and the life-history strategies of microorganisms regulate microbial activity and carbon use is poorly understood. There is still a lack of mechanistic and spatially explicit understanding of how pore size, resource distribution, and microbial life-history strategies jointly regulate microbial processing of resources and the resulting carbon dynamics. The two microbial traits that are the most likely to influence C use in such heterogeneous systems are related to the intrinsic abilities of the microbes to use the C available to them and their ability to gain access to C substrates.

The different microenvironments that occur in the pore network have been classified according to, among others, resource availability (Li et al., 2024). The differences in conditions, naturally, exert selective pressures on the microbial communities which are more adapted to high or low levels of resource availability. The r/K selection theory provides a simple and widely used framework for interpreting the dynamics and distribution of soil microorganisms (Fierer et al., 2007; Peng et al., 2022). While the r- and K-selection framework does not capture the full complexity of microbial life-history strategies (Reznick et al., 2002), it provides a simple and intuitive way to represent key ecological trade-offs. According to this classification scheme, r-strategists favour resource-rich conditions (copiotrophic species) but perform poorly when nutrient availability is low, while K-strategists grow more slowly but perform relatively better in resource-poor environments (oligotrophic species) (Fierer et al., 2007; Gao et al., 2025; Zheng et al., 2024). Therefore, the r/K selection theory is likely appropriate for this kind of system.

Motility is another trait that allows microorganisms to adapt to their microenvironment: the ability to move in the porous soil environment can confer a selective advantage under certain conditions. Although direct observations of microbial motility in unsaturated soils remain technically challenging due to the opacity and complexity of soil (Wang and Or, 2010), several studies indicate that soil moisture and pore network structure control microbial motility by regulating water film continuity and spatial connectivity within the pore space (Barton and Ford, 1997; Chang et al., 2009; Or et al., 2007; Young and Crawford, 2004). In particular, the presence of continuous water films is necessary for flagellar motility, which limits its expression in dry soils. As motility is energetically costly, its prevalence also appears to be modulated by the availability of organic carbon, an essential resource for microbial metabolism. Thus, carbon-rich environments, such as rhizospheres, tend to favour motile bacteria, as evidenced by higher levels of flagellar genes detected in these areas (Ramoneda et al., 2024). Conversely, in more resource-poor or arid environments, motility is often less prevalent. However, the role of pore-scale geometry, particularly pore size distribution and connectivity, in modulating the costs and benefits of motility remains poorly quantified. In particular, it is still unclear how physical constraints and spatial resource heterogeneity interact to determine when motility enhances microbial growth and carbon use.

The modelling of soil processes has made great strides due to the development of spatially explicit, mechanistic approaches that account for the physical structure of soil (Ray et al., 2017; Ritschel and Totsche, 2019; Rötzer et al., 2026; Zech et al., 2022). However, these models focus primarily on physical heterogeneity and do not always account for the functional diversity of microbial communities. The integration of realistic soil structure with explicit microbial ecological dynamics remains a major challenge (Baveye et al., 2011; Otten et al., 2001; Pot et al., 2021). With some notable exceptions (Allison, 2005), approaches tend to separate these aspects: models focused on microbial processes often consider homogeneous environments, while models that account for soil heterogeneity generally ignore microbial traits

and interactions (Panikov, 1999). This disconnection impairs our understanding of the mechanisms underlying microbial carbon use in structured environments. Here, we use a cellular automaton framework which explicitly represents spatial structure and microbial interactions that are based on local rules, in order to determine how microbial traits affect C processing under different local environmental conditions. The framework includes distinctive physiological traits for r- and K-strategists, different types of motility, resource distributions and two fixed moisture conditions. The spatial structure of the environment was derived from X-ray tomographic images of soil.

2 Material and methods

A cellular automaton is a discrete mathematical model composed of a regular grid of units, each of which can adopt a finite number of states. The system evolves over time in synchronous steps, where the future state of each unit is determined by its current state and that of its neighboring unit, according to a set of predefined transition rules (Wolfram, 1990). In this study, each grid unit represents a microscopic spatial unit. Explicit spatial interactions can occur between microbes, as well as between microbes and organic substrates. The system is based on two coupled matrices of 100×100 cells (pixels).

The state matrix identifies the nature of each grid unit in the automaton. Eight distinct states of the grid cells are taken into account, corresponding to different soil components or biological types: (1) solid phase of the soil, (2) air-filled porosity, (3) water-filled porosity, (4) carbon resources, (5) motile r-strategists, (6) immobile r-strategists, (7) motile K-strategists, and (8) immobile K-strategists (Table S1 in the Supplement). These eight states are mutually exclusive: each grid unit is assigned exactly one state at each time step.

The resource matrix quantifies the amount of resources associated with each grid unit, when applicable, and is used to monitor carbon flows in the system. It is coupled to the state matrix in that it only takes non-zero values for cells whose state is "carbon resource" (representing the quantity of organic carbon available at that location) or one of the four microbial states (representing the internal carbon reserve of the corresponding cell, used to fuel maintenance, motility, and reproduction). Cells in the solid phase, air-filled porosity, or water-filled porosity states are assigned a resource value of zero, as no carbon stock is associated with them. This dual architecture makes it possible to model the system's spatial structure, which remains strictly discrete, separately from its resource content, which varies continuously within the constraints imposed by the discrete state of each cell.

2.1 Initialization

X-ray micro-tomographic images of a Luvisol (resolution 19 µm), obtained from the Soil Structure Library (https://structurelib.ufz.de/lit/, last access: 5 March 2026; Weller et al., 2022) in the form of a TIFF image stack, were used to create the state matrix.

2.1.1 Soil images

Ten regions (100×100 pixels) were randomly selected from different images of the image stacks. If a region did not contain any usable pores (i.e., no empty space or, conversely, no solid matter), it was discarded and another one was extracted. The 10 image regions were thresholded using the Otsu method to separate pores and solid phases (Smet et al., 2018).

2.1.2 Optimization of pore connectivity

Since image resolution tends to obscure the narrower pores and reduce the connectivity of the porous network, we applied Bresenham's algorithm to the 10 thresholded images in order to establish connections between physically close but unconnected pores (Bresenham, 1965). This method establishes connections based on the relative distance, spatial orientation, and surrounding configuration of the pores (Bresenham, 1965).

2.1.3 Pore classification and characterization

The classification and characterization of pores in the thresholded images consisted of a sequence of steps that began with a morphological erosion to extract the skeleton of the pore network. The pores were then classified based on the distance between each pixel of the skeleton and the nearest solid phase pixel. Pores for which the skeleton pixels were at a distance of less than 4 pixels (4 µm) were considered small pores (small, S). Other pores were classified as large pores (large, L). The images contained on average 22.89 ± 2.13 % macroporosity and 17.09 ± 1.61 % microporosity.

2.1.4 Distribution of resources within the pore network

All resources were placed either in small (S) or large (L) pores as defined before (Fig. 1). The resources were distributed so that the concentration of resources in each pore size class was the same. The resources occupied 2.83 % of the surface area of the 2D matrix, which is less than what is generally found in soil (5 %–25 % soil volume (Hudson, 1994; Libohova et al., 2018). However, all the resources were placed in the pore network and were therefore readily available to microbial decomposers, which is not the case in soil. Generally, < 20 % is readily available in soil (Bongiorno et al., 2019; Haynes, 2005; McLauchlan and Hobbie, 2004). The amount of resources added therefore approximated the amount of readily available resources found in soils. For this study, each resource unit contained 100 resource points, however, other simulations have been carried out to investigate

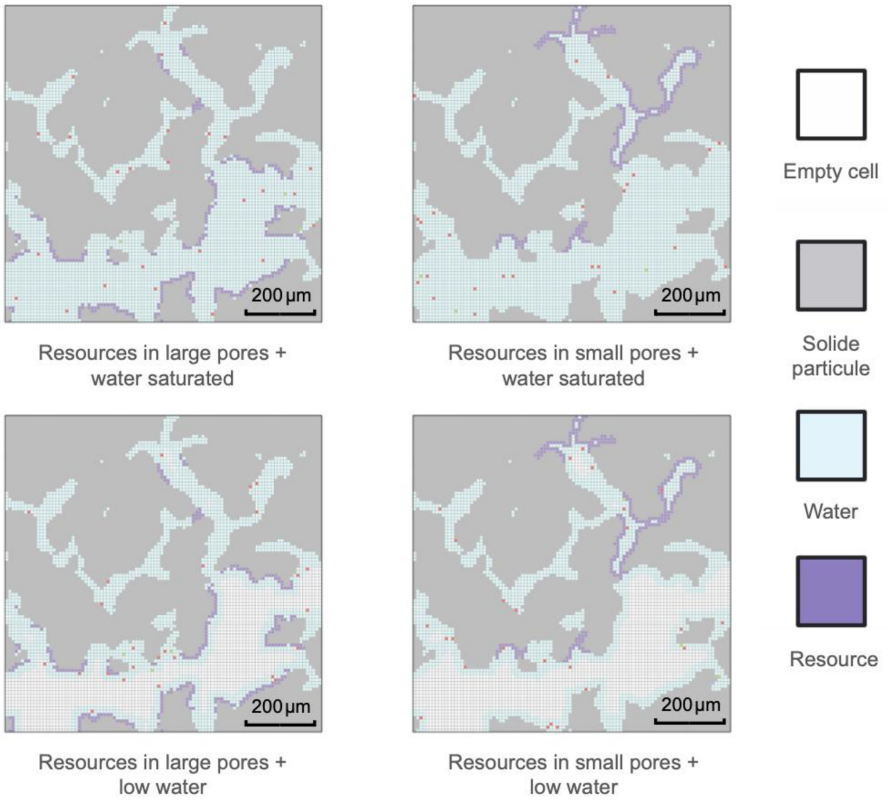


Figure 1. Diagram showing the four initial conditions of moisture and resource distribution for a given matrix. The isolated green and red pixels that are barely visible on the grids represent microbial cells randomly placed at the start of each simulation.

the effect of a change in the number of points contained within the resource units (Fig. S8).

2.1.5 Moisture management in matrices

Each matrix was assigned a specific moisture level. Moisture was distributed throughout the pore space by adding a layer of water pixels next to the solid surface. Further layers of moisture pixels were then added in succession until the desired moisture level was reached. This process is akin to morphological dilation and results in the narrower pores being filled first. In addition, dilation ensures the connectivity of the pore network from the start of the simulations without creating heterogeneity between large and small pores (Fig. 1). This study focuses on comparisons between two specific humidity levels. In the supplementary material, other humidity levels have been examined.

2.2 General automaton rules

The cellular automaton model used here is based on a set of deterministic rules applied synchronously at each simulation time step, modifying both the state matrix and the resource matrix. In each matrix, only water-filled pore grid units, resources grid units and microbial cells can change state. Within a simulation, solid phase grid units and empty pores are immutable and represent the inherent constraints of a particular matrix (Fig. 2).

The amount of resources in the system is defined at the start of the simulation in the form of resource elements, 100 of which is assigned to each resource grid unit. Resources can diffuse from their initial locations in the matrix according to a propagation model that follows Moore's neighbourhood (eight adjacent grid unit; Cellular Automata – The Moore neighbourhood, 2026). This diffusion occurs along concentration gradients, with resources spreading from resource-rich to resource-poor zones. At each iteration i, resources diffuse if the resource content of a grid unit is above a threshold value. Fixed amounts of resources are distributed from resource-rich grid units to neighbouring grid units with lower resource contents, up to a maximum diffusion rate. The change in resources in a water or resource grid element (x, y) can therefore be written as:

$$\text{Resource}^{i+1}_{(\text{resource } x,y)} = \text{Resource}^{i}_{(\text{resource } x,y)} - \sum_{m,n\in\{-1,0,1\}} T^{i}_{(x+m,y+n)} \quad (1)$$

where $T^{i}_{(x+m,y+n)}$ denotes the amount of resources transferred between cell (x, y) and its neighbour $(x+m, y+n)$

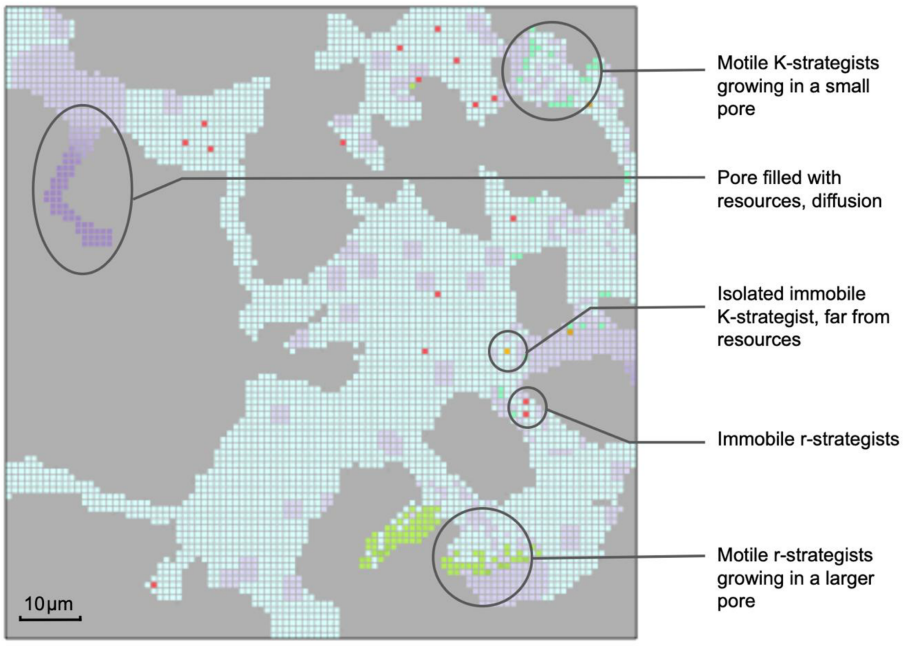


Figure 2. Image taken from one of the simulations showing strategists r and K present simultaneously in the matrix (iteration 50). The different colors represent the various states of the units: light blue for water, gray for the solid phase of the soil, purple for resources (with the intensity of the purple indicating the concentration of resources), green for mobile cells, and red/orange for immobile cells.

during iteration i. By convention, T^i is positive when (x, y) is more resource-rich than its neighbour $(x+m, y+n)$, i.e., resources flow out of (x, y), and negative when the reverse holds. This transfer is constrained by a diffusion threshold (donor eligibility), such that a non-zero transfer occurs only if $\text{Resource}(x, y) \neq \text{Resource}(x+m, y+n)$, and by a fixed diffusion rate (maximum transfer per neighbour), such that the richer of the two cells loses a constant quantity to the poorer one rather than a gradient-proportional amount. This produces a stepwise and locally asymmetric redistribution process, leading to a gradual homogenization of resource distribution across the matrix without reaching instantaneous equilibrium.

Microbial cells take up all resources that are present in the grid unit that they occupy. The resources arrive in the grid unit by diffusion or were already present when a motile microbial cell came to occupy the grid unit.

At the end of each iteration, the total accumulated resource content stored in a microbial cell is used as an internal state variable ("resource points") that determines its physiological status. This accumulated pool is then compared to the predefined thresholds that govern microbial processes such as maintenance, survival, reproduction, or mortality.

The different types of microbial cells (Table 1) transition between three states (growth, maintenance or death), depending on resource availability. The transitions are regulated by three critical resource thresholds. The maintenance threshold (Sd) triggers a state of reduced metabolism when resources become scarce. During maintenance, cells do not move or reproduce. If the resource scarcity persists and falls below the mortality threshold (Sm < Sd), the microbial cell dies and the remaining resource is transferred to the available resource pool. Conversely, the accumulation of resource above the reproduction threshold (Sr) activates cell division, in which a new cell of the same type appears in any of the eight adjacent aqueous grid units. The parent cell invests a significant proportion of its resource (25 % to 50 % depending on the microbial strategy) in this process according to the formula :

$$\text{Resource}^{i+1}_{(\text{parent } x,y)} = \text{Resource}^{i}_{(\text{parent } x,y)} - \text{Resource}^{i+1}_{(\text{descendant } x,y)} \quad (2)$$

where Cr represents the fixed metabolic cost of reproduction (Table 1).

The location of the descendant cell is chosen randomly among the set of available neighboring cells that can be occupied (i.e., empty or otherwise permissible states depending on the model rules). If no suitable cell is available in the local neighborhood, reproduction does not occur during that iteration and is postponed until space becomes available. In practice, this situation is rare due to the spatial structure and occupancy dynamics of the cellular automaton.

The reproductive costs vary among microbial cell types, the cost being higher for K-strategists, which invest in fewer, larger, and more resource-rich offspring or cellular structures optimized for survival under stable but competitive conditions, rather than in the rapid, low-cost proliferation favored

Table 1. Different cell types present in the simulations, and the associated resource costs and thresholds.

Cell type	Motility	Motility cost	Maintenance cost	Dormancy threshold	Mortality threshold	Reproduction cost (Cr)	Reproduction threshold
r-strategist cells	Mobile	1	1	60	30	55	100
	Immobile	0	1	60	30	55	100
K-strategist cells	Mobile	5	3	60	30	70	250
	Immobile	0	3	60	30	70	250

by r-strategists. This trade-off between investment per offspring and reproductive rate also extends to resource acquisition strategy, which itself carries a cost that differs between motile and immobile cell types.

Motile cells can search for and exploit available resources within a configurable perception radius R. Motile cells move at a speed of one grid unit per iteration towards the nearest and most resource-concentrated resource grid unit within their perception radius. Due to the cost of motility, motile cells focus only on resources with a resource content above a defined threshold equal to 5 resource elements (Table 1). The cost of motility (Cm) is deducted for each move according to: $\text{Resource}(t+1) = \text{Resource}(t) - \text{Cm}$. The inability of mobile cells to anticipate obstacles, such as pore walls, when moving toward the nearest resources introduces a realistic constraint that limits their effectiveness in complex environments. Immobile cells rely entirely on the diffusion of resources to acquire the resource and matter necessary for maintenance and growth. This resource acquisition strategy is energetically more economical, due to the absence of motility costs.

2.3 Simulation runs

For each of the 10 pore-space images, four distinct initial conditions were generated by combining two moisture levels (water-saturated and low-water conditions) with two resource spatial distributions (resources located either in large pores or in small pores). This results in a total of 40 distinct initial matrices ($= 10$ images $\times$ 2 moisture levels $\times$ 2 resource distributions). For each initial matrix, simulations were then performed with different microbial community configurations, combining two initial microbial densities (low: 23 cells, and high: 56 cells) and three microbial diversity treatments (r-strategists only, K-strategists only, and mixed r + K communities).

Each unique combination of initial matrix and microbial configuration was replicated 20 times and simulated over 200 iterations. This full factorial design resulted in a total of 4800 simulations runs.

2.4 Sensitivity analysis of the model

In addition to the simulations presented above, analyses were performed to establish the sensitivity of the model to (1) matrix moisture, (2) initial resource concentration, and (3) the parameters governing the r- and K-strategies. Details of the methods and results obtained for these additional simulations are presented in the supplementary data.

2.5 Model parametrisation and realism

At the beginning of the simulations, microbial biomass represented between 9.0 % (low microbial density) and 16.5 % (high microbial density) of total soil organic carbon (SOC). These values were chosen as they are representative of the rhizosphere, a highly active soil compartment characterized by elevated microbial densities relative to total organic carbon (Zhao et al., 2022). Although microbial biomass is often reported to represent a smaller fraction of SOC in bulk soils, typically reaching up to ~ 6 % in field measurements (He et al., 2021), estimates based on fumigation–incubation methods indicate microbial biomass carbon contents ranging from 300 to 1200 mg C kg^{-1} in natural silt–clay soils (Franzluebbers et al., 1994; Jenkinson and Powlson, 1976; Sparling and West, 1988), corresponding to approximately 1.5 %–12 % SOC in soils containing 1 %–2 % total organic carbon. The values used in the present model therefore fall within, or slightly above, the upper range reported in the literature, consistent with a focus on the rhizosphere rather than bulk soil. Within the model, the use of relatively high initial microbial densities aimed to ensure the establishment and persistence of microbial populations over the simulation period, while allowing a representative distribution of different functional types across heterogeneous microenvironments (pores of varying size and resource availability). Although the model assumes an identical total amount of carbon between pore types, the differential accessibility generated by diffusion constraints and spatial geometry conceptually reproduces empirical gradients. Cells were initially distributed randomly in space to avoid imposing predefined spatial advantages among microbial types (mobile vs. immobile) and life-history strategies (r vs. K), thereby allowing differences in colonization dynamics to emerge from intrinsic traits and interactions.

In the model, the recycling rate of microbial biomass (cellular resource) was set to 100 %, meaning that the entire resource content of dead cells was instantaneously transferred to the pool of assimilable resources. This assumption implies

an immediate decomposition of cellular structures and the absence of a non-assimilable organic matter compartment. Empirical studies indicate that microbial biomass recycling efficiency in soils is much lower. Although microbes are able to feed on microbial necromass, recycling efficiencies rarely exceed 12 % (Kästner et al., 2021), and microbial necromass can constitute more than half of total soil organic carbon stocks (Liang et al., 2019). The use of a 100 % recycling rate therefore does not aim to represent realistic microbial necromass processing, but rather reflects a deliberate structural simplification of the model. All cellular resource is assumed to be potentially accessible to other microbes, corresponding to an idealized and instantaneous transformation of biomass into assimilable resources. As a consequence, the model accelerates carbon transformation processes compared to real soil systems and likely overestimates the efficiency and speed of microbial biomass recycling. This limitation should be kept in mind when interpreting model outcomes.

2.6 Carbon use efficiency calculation

In the model, carbon use by microbial communities is described through their carbon use efficiency (CUE), a widely used metric in soil microbial ecology that reflects how efficiently microorganisms convert the carbon they take up into new biomass, as opposed to losing it through respiration. A high CUE indicates that a large proportion of assimilated carbon is invested in growth, whereas a low CUE indicates that most of the carbon taken up is respired to meet maintenance and metabolic costs, with proportionally less contributing to biomass production. CUE is computed at each iteration based on carbon fluxes at the level of the microbial community. The total carbon uptake by microbes includes both the portion converted into biomass (growth) and the portion lost through respiratory processes (maintenance and metabolic costs). CUE is therefore defined as the ratio of carbon allocated to biomass to total carbon uptake: $\mathrm{CUE} = (\text{carbon allocated to biomass})/(\text{total carbon uptake})$. This ratio made it possible to assess the influence of multiple factors on the metabolic efficiency of microbial communities: resource location, water regime, adaptive strategies, and microbial motility.

2.7 Statistical analysis

Analysis of microtomographic images to extract pore-space images and initialize the simulation matrices was carried out in Python while the cellular automaton model itself was developed in R. Python was only used during the preprocessing stage to extract pore-space images and initialize the simulation matrices from the image data. The spatial simulations and visualizations were implemented using custom R scripts rather than relying on an existing cellular automaton framework or dedicated spatial modeling library. The code used for this work can be found at https://doi.org/10.5281/zenodo.21336136 (Maelmstr., 2026) and model current development is available at https://github.com/Maelmstr/soil-cellular-automaton (last access: 10 October 2026).

All statistical analyses were performed using R (R, 2026). The demography of microbial populations, their use of resources for maintenance, growth and movement, and the temporal dynamics of resources were monitored for each simulation. The first 25 iterations of each simulation were treated as a warm-up phase and excluded from CUE calculations, in order to limit the influence of the random initial spatial placement of microbial cells on the resulting efficiency estimates. During this early period, the dominant process is the spatial redistribution of mobile cells toward accessible resource-rich areas, with population density curves showing that microbial populations already increase rapidly within the first iterations. As a result, the resource distribution at iteration 25 is no longer strictly equivalent to the initial condition, but this shift was expected and intentional: our aim was to assess microbial efficiency once the initial, largely arbitrary spatial configuration had reorganized into a more ecologically meaningful pattern shaped by microbial movement and local resource accessibility, rather than to capture the transient dynamics from initial conditions. Since this warm-up period was applied uniformly across all simulations, any resulting differences in resource availability at iteration 25 affect all treatments comparably, so that relative comparisons among treatments remain valid. Furthermore, because the warm-up phase represents only a small fraction of the total simulation length, its exclusion is expected to have a limited effect on the overall CUE estimates.

Analysis of the calculated CUE was done using analysis of variance (ANOVA), with location of resources in pore size, moisture condition, and mobility as fixed factors. Tukey Honest Significant Differences post-hoc pairwise comparisons were then performed to account for multiple comparisons.

3 Results

3.1 Populations dynamics

The initial microbial cell density had no effect on the population dynamics profiles of r- or K-strategists and therefore the results for the more abundant initial cell numbers are presented in the main text (Fig. 3) and those the less abundant initial populations are shown in the Supplement (Fig. S1). The mortality of immobile K-strategists was very high during the first 50 iterations (Fig. 3a) and was directly linked to their initial position in the matrix: if they were positioned too far from resources, the diffusion rates of resources were not sufficiently high to satisfy their energetic requirements for survival. Compared to immobile K-strategists, immobile r-strategists (Fig. 3b) reproduced more easily, due to their lower reproduction threshold. As a result, a small population

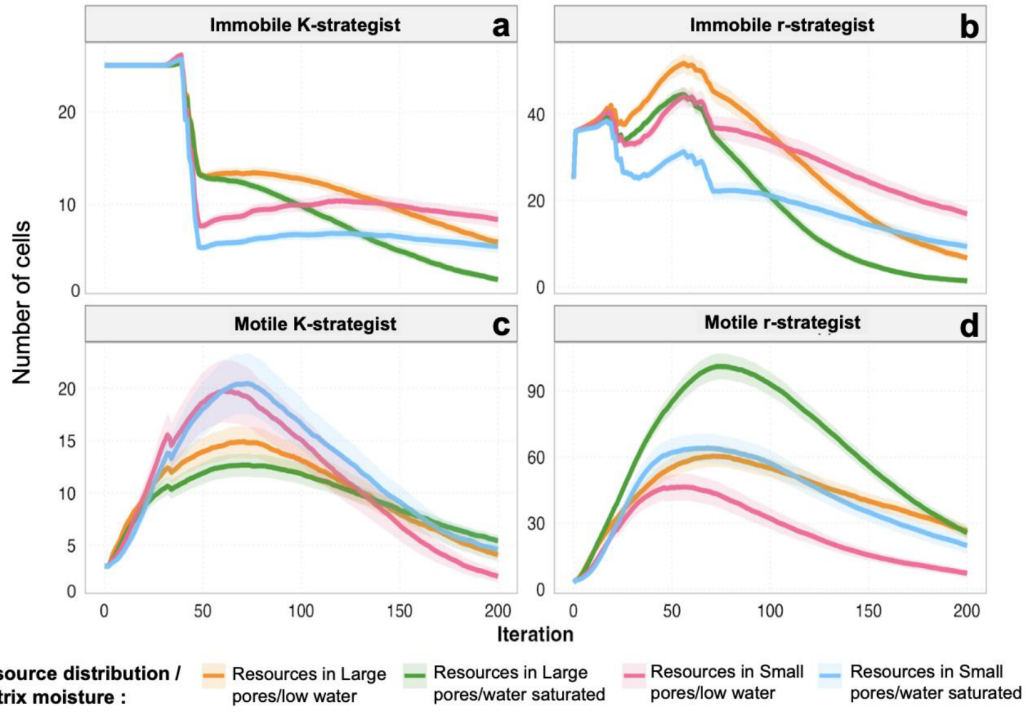


Figure 3. Number of motile and immobile cells with either r- or K-strategies in simulations with an initial population size of 56 cells (50 immobile and 6 motile). The results of simulations with initial populations of 28 initial cells were similar and are available in the Supplement (Fig. S1). The colours refer to the different initial matrix configurations, where, resources were distributed in the large pores (orange and green) or in the small pores (pink and blue). Matrices were either saturated with water (green and blue) or low water (pink and orange). Note that the *y* axis scales are different. The shadows correspond to the standard deviation (10 images and 20 repetitions).

peak was observed between iterations 50 and 80 (Fig. 3b). Thereafter, resource limitation caused a decrease in population size as cell death rates surpassed reproduction rates. It is interesting to note that the largest immobile populations were found in the large pores. However, immobile populations persisted longer in small pores, especially at low moisture levels. The most unfavourable initial configuration for the persistence of immobile populations over time was when resources were in large, water-saturated pores.

The population dynamics of the motile populations showed an initial increase in size during the first 50 iterations (Fig. 3), which was followed by a decrease, as the populations became resource limited. The results observed for motile populations differed according to the life strategy: the population of r-strategists increased to over 100 cells/matrix while the populations of K-strategists remained more modest at fewer than 40 cells/matrix (Fig. 3c). The populations of K-strategists reached a maximum when the resources were located in small pores, whereas r-strategist populations thrived when resources were in large, water-saturated pores. Neither r- nor K-strategists thrived in the other's preferred environments. The least favourable situation for motile r-strategists was when resources were in small pores with low water content. In this scenario, the environment impeded motility, thus reducing both the rate at which resources were acquired and the reproduction rate.

Simulations in which both r- and K-strategists were present together showed that competition affected both populations, whether they were motile or immobile, from approximately the 40th iteration onwards, resulting in decreases in population size (Fig. 4). This was due to resources becoming more limited relative to the needs of the populations. The competitive interactions resulted in r-strategists dominating the matrix. As stated above, the same general dynamics were observed with a larger initial cell supply (56 r-strategists and 56 K-strategists) (Fig. S2).

3.2 Microbial carbon use efficiency

The CUE differed markedly among microbial strategies and initial community sizes (Fig. 5). Overall, communities dominated by K-strategists exhibited higher CUE than either those dominated by r-strategists or mixed communities. The highest CUE values were observed in K-strategist communities with low initial cell densities. In contrast, r-strategist communities consistently showed a lower CUE under comparable conditions (Tukey: $P < 0.001$).

Increasing the initial number of cells led to a decrease in CUE for both r- and K-strategist communities, indicating a

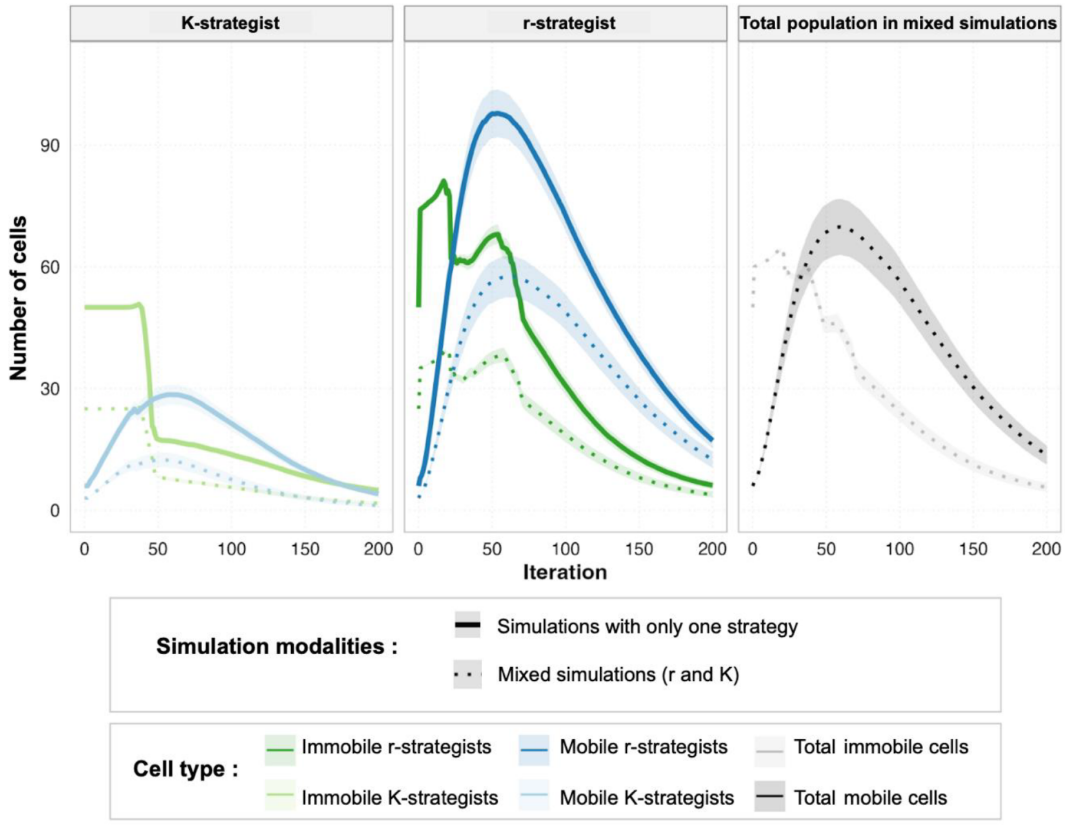


Figure 4. Simulations showing the effects of competition between r- and K-strategists. K-strategists, r-strategists and total cell populations in which r-strategists (28 cells) and K-strategists (28) were present together in the same matrix. The solid lines show simulations without competition which correspond to situations with K strategists only (25 immobile and 3 motile) and r strategists only (25 motile and 3 immobile) respectively. The dashed lines show the results of simulations with competition, where r- and K-strategists were both present in the matrices. The grey curve in the third panel is the sum of the immobile K and r cells in the previous two panels. The black curve on the third panel is the sum of moving K and r strategists on the previous two facets.

negative effect of initial density on carbon use efficiency. Mixed communities composed of both r- and K-strategists exhibited the lowest CUE values across all scenarios. Statistical support for these effects was provided in Fig. S3.

In addition to the effects of metabolic strategy and the initial cell numbers, the location of resources in specific pores also had significant effects ($F = 101.53$; $P < 0.001$), as did microbial cell motility ($F = 138.89$; $P < 0.001$) and their interaction ($F = 328.03$; $P < 0.001$).

Firstly, higher CUE values (0.40 ± 0.04 for K cells and 0.39 ± 0.04 for r cells) were always obtained for immobile cells under low water conditions. The next highest, but significantly lower (Tukey: $P < 0.001$), CUE values were obtained when resources were in water saturated small pores (0.36 ± 0.07 for K cells and 0.35 ± 0.04 for r cells). When the resources were in large pores, immobile cells showed the lowest CUE, in particular under water-saturated conditions (0.24 ± 0.04 for K cells and 0.23 ± 0.02 for r cells).

The motile cells with the largest CUE were observed in the large pores (Fig. 5). In the case of motile K-strategists, these were large, water-saturated pores (CUE $= 0.49 \pm 0.05$), while in the case of motile r-strategists, large pores, whether water-saturated or not, were indifferently associated with the highest CUE (Tukey: $P = 0.50$). In contrast to what was described for immobile cells, motile cells in small pores had reduced CUE, with the lowest CUE found in small pores with low water content (CUE $= 0.28 \pm 0.04$ for K-strategists and CUE $= 0.31 \pm 0.04$ for r cells).

The simulations with both r and K strategists enabled us to determine the effect of competition between the different cell types on CUE. Increasing the initial cell density significantly reduced CUE, the strategy of the cells also had a significant effect, with K-strategists having higher CUE values. The K-strategist cells were more sensitive to the presence of r-strategists. In contrast, the CUE of r-strategists was less sensitive to the presence of K-strategists in the matrices. This competitive effect was largely modulated by the initial conditions of the matrices, the size of the resource distribution pores, but also humidity (Fig. 6).

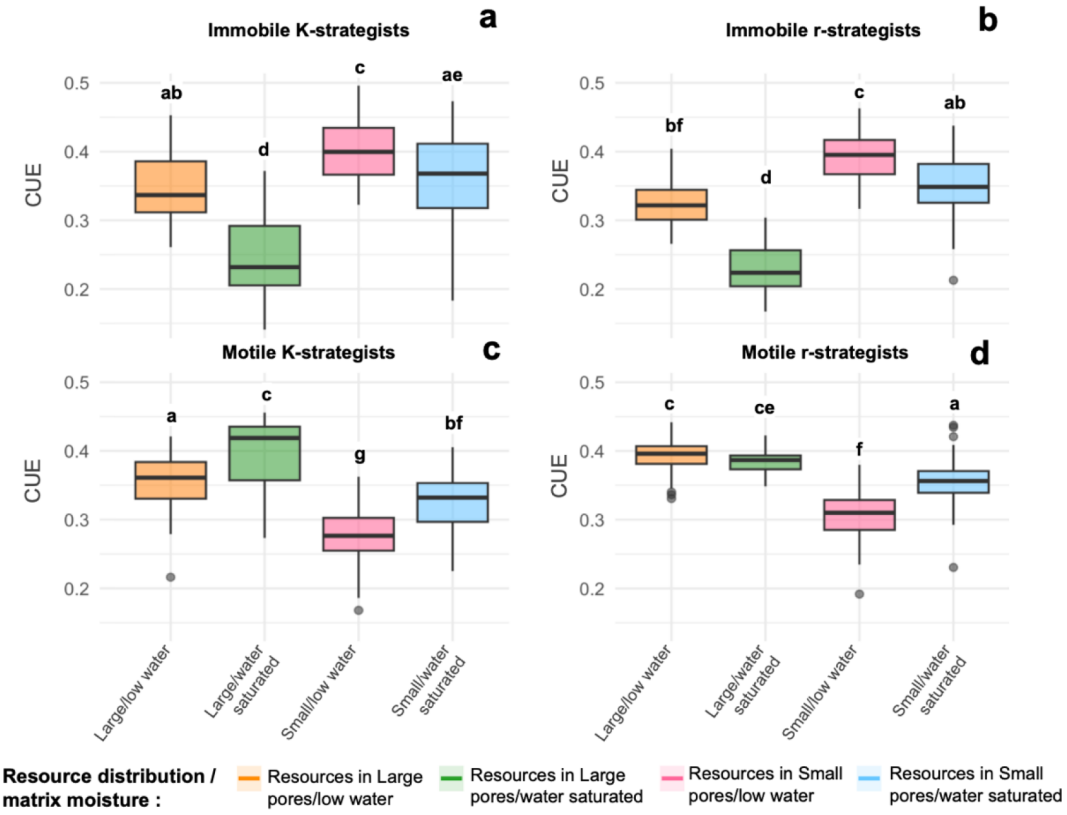


Figure 5. Panel graph showing average CUE for each different cell type. Average CUE values were calculated from the 25th iteration onwards, in order to avoid the uncertainty associated with the population fluctuations at the beginning of the simulations. This analysis took into account the 5 initial scenarios with r- and K-strategists separately for the two initial cell densities (28 and 56), as well as the mixed scenario with r- and K-strategists present together in the simulations. The colours used refer to the different initial matrix configurations. In orange and green, resources were distributed in the large pores, and in pink and blue, resources were distributed in the small pores. Green and blue refer to matrices saturated with water, and pink and orange to matrices with a one-pixel water film covering the solid phase of the soil and the resources. Letters on the figure refer to statistical differences between groups (Tuckey).

The results showed that the initial configurations of the matrix had different effects on the cells; the two most distinct configurations were those in which the pore network was saturated with water, with resources distributed only in the large pores (Fig. 6a), and in which water was limited and resources were found only in the small pores. When the pore network was water-saturated and resources were only in large pores (Fig. 6a), motile r-strategists were not affected by increasing cell density in the initial state (Tukey: $P = 0.32$), nor by competition with motile K-strategies in the mixed situation (Tukey: $P = 0.99$). However, this was not the case for motile K-strategists, whose CUE was reduced when there were motile r-strategists in the matrix (Tukey: $P < 0.001$). In the case of immobile cells, r-strategists were affected at greater initial cell densities (Tukey: $P < 0.001$), regardless of whether these were r- or K-strategists (Tukey: $P = 0.36$). The CUE of immobile K-strategists was reduced when the initial number of K-strategists was high (Tukey: $P < 0.001$), and reduced further when in the presence of r-strategists (Tukey: $P < 0.001$).

When resource was in small pores in low water conditions (Fig. 6b), the CUE of r-strategists was unaffected by the increase in initial cell density (Tukey HSD: $P = 0.001$), and did not differ from the CUE of K-strategists (Tukey: $P = 0.98$). The effects were different for motile K-strategists, whose CUE was not affected by high initial densities of K-strategists (Tukey: $P = 0.99$), but were affected when in the presence of motile r-cells (Tukey: $P < 0.001$). As far as immobile cells are concerned, the effects were identical for both cell strategies, with the CUE lowered by higher initial cell densities, regardless of their identity.

3.3 Sensitivity analysis, moisture, resource concentration, and life-history parameters

Additional simulations were performed to test the sensitivity of the model to moisture level, initial resource concentration, and the individual parameters governing r- and K-strategists life histories.

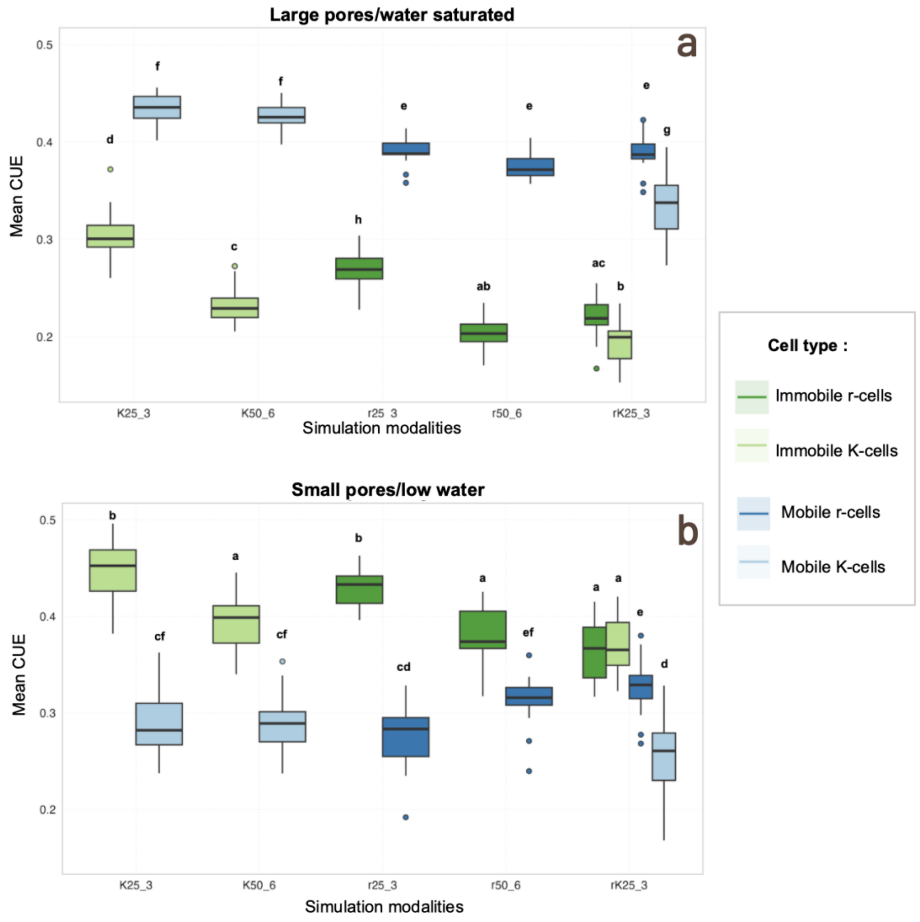


Figure 6. Graphical panel showing the mean CUE in all the different initial matrix configurations, resources distributed in large pores or small pores with or without water saturation. Colours refer to the different cell types present in the matrices. K25_3 and K50_6 correspond to situations with K strategists only (25 immobile K cells and 3 motile K cells or 50 motile K cells and 6 immobile K cells respectively). r25_3 and r50_6 correspond to situations with r strategists only (25 immobile r cells and 3 motile r cells or 50 motile r cells and 6 immobile r cells respectively). rK25_3 show the results of simulations with competition, where r and K cells have been added jointly to the matrices (25 immotile K cells and 3 motile K cells with 25 motile r cells and 3 immobile r cells). The letters correspond to the statistical groups given by a Tuckey analysis, for each panel graph, the groups have been calculated separately.

Cell sensitivity to moisture was only detectable at the lowest humidity levels tested; above a water film thickness of 6 pixels, most pores were nearly saturated, reducing the differences observed between conditions. When resources were located in large pores, moisture had no significant effect on either motile or immobile cell populations or their CUE. In contrast, when resources were distributed in small pores, moisture had a marked effect: at the lowest moisture level, immobile cells reached higher mean population sizes (26.3 ± 12.3) than motile cells (12.8 ± 8.6, $P < 0.001$), and immobile CUE (0.41 ± 0.06) exceeded motile CUE (0.28 ± 0.12, $P < 0.001$). This pattern was reversed at higher moisture levels, where motile cells reached higher mean populations (52.4 ± 23.6) and CUE (0.41 ± 0.10, $P < 0.001$), while immobile populations (16.3 ± 15.3) and CUE (0.20 ± 0.15) decreased ($P < 0.001$) (Fig. S7).

Varying the initial resource concentration (10–300 resource units per resource cell) showed that at low concentrations (10–25 units), immobile cells reached higher mean populations than motile cells ($P < 0.0001$). As resource concentration increased, motile cells increasingly outperformed immobile cells, particularly when resources were located in large pores ($P < 0.0001$). CUE tended to be stable above a threshold concentration: motile cell CUE plateaued rapidly at 0.38 ± 0.09 in large pores, while immobile cell CUE continued to increase with resource concentration, from 0.02 ± 0.04 to 0.32 ± 0.07. In small pores, CUE dynamics were similar between motile and immobile cells (Fig. S8).

Systematic variation of the four parameters governing r- and K-strategist life histories (motility cost, maintenance cost, reproduction cost, reproduction threshold) showed that pore size had a stronger effect on CUE ($F = 1149.13$, $P < 0.001$) than any individual life-history parameter, and also

altered which parameter combinations maximised CUE. In large pores, maintenance cost was the dominant factor, explaining more than 70 % of the variance in CUE for both motile and immobile cells. In small pores, reproduction threshold was the dominant factor, explaining more than 45 % of the variance. Correlation analysis showed that the canonical r (0000) and K (1111) parameter combinations were never the most divergent in their effect on CUE, indicating non-additive interactions among parameters; these interactions accounted for a larger share of the variance in small pores than in large pores (Figs. S9–S14).

Full methodological details and statistical outputs for all sensitivity analyses are provided in the Supplementary Material.

4 Discussion

4.1 Comparison of the model with other cellular automata and spatially explicit approaches

As outlined in the introduction, spatially explicit, mechanistic models have considerably advanced our understanding of soil physical structure (Ray et al., 2017; Ritschel and Totsche, 2019; Rötzer et al., 2026; Zech et al., 2022). However, these approaches have largely developed along two separate lines: models that prioritize the physical heterogeneity of the soil matrix, generally without resolving microbial trait diversity, and trait-based microbial models that capture life-history strategies but are typically developed under homogeneous or implicit spatial conditions, with few frameworks operating at the interface of the two. A notable exception is the DEMENT model (Allison, 2012), which combines microbial trait diversity with spatially explicit dynamics; however, DEMENT is typically implemented on simplified or generic spatial grids rather than on pore-scale structures derived from empirical imaging data. The framework presented here contributes to bridging this gap by explicitly coupling a pore-scale spatial structure, derived from X-ray tomographic imaging, with microbial functional traits (r- and K-strategists, distinct motility types) and local, rule-based interactions. Compared with models that prioritize physical heterogeneity but omit microbial trait diversity (e.g., Ray et al., 2017; Ritschel and Totsche, 2019; Zech et al., 2022), our approach makes it possible to examine how microbial life-history strategies interact with, and are constrained by, realistic pore-scale structure. Conversely, compared with trait-based microbial models developed under homogeneous conditions (Panikov, 1999), our framework allows resource accessibility and microbial performance to emerge from explicit spatial constraints rather than being assumed uniform. At the same time, this focus on spatial structure and microbial traits comes at the cost of the biochemical and physiological detail found in more mechanistic models suggesting that future work coupling these complementary modeling traditions could yield a more comprehensive representation of microbial carbon cycling in structured soils.

4.2 Realism of model outputs

4.2.1 Microbial dynamics and cells characteristics

The population dynamics observed for motile cells, which were characterized by rapid growth following resource inputs, high turnover, and strong temporal fluctuations are consistent with rhizosphere population dynamics described in the literature (Darrah, 1991; Newman and Watson, 1977). We observed that microbial growth was limited by the supply of organic substrate, so an increase in microbial cell populations was associated with greater consumption of available resources in the environment, led to resource limitation and subsequently to the collapse of microbial populations. In the case of immobile cells, the population dynamics observed were more dependent on competition with motile cells for resources.

Although all cells were assumed to have the same size (1 pixel = 1 µm), r- and K-strategists were parameterized with different overall costs related to maintenance, motility and reproduction, with K-strategists incurring higher costs and higher reproduction thresholds. This choice was intended as a simplified proxy for the effect of cell size on these costs, rather than an explicit representation of size variation: theoretical predictions indicate that the various costs associated with cellular life (motility, maintenance, reproduction) are closely linked to cell size (Kempes et al., 2017), with motility in particular depending heavily on cell size, to the point that directed motility is assumed to be inefficient and effectively absent below a critical volume (Dusenbery, 1997). In small microorganisms, motility can represent an energy cost comparable to, or even greater than, maintenance costs (Kempes et al., 2017). To assess the impact of these trade-offs directly, we ran supplementary simulations in which costs were varied arbitrarily around the r- and K-strategist values, allowing us to examine how differences in resource allocation influence microbial dynamics in a porous space (Fig. S4).

4.2.2 Model scales

While the spatial scale of the model is explicitly defined, translating the temporal dimension into real-world units is less straightforward, owing to the discrete and rule-based nature of the cellular automaton framework. In this model, one iteration represents a generic update step encompassing resource diffusion, microbial uptake, maintenance costs, movement, and reproduction, rather than a directly measurable unit of real time such as hours or days. It should therefore be interpreted as a composite step integrating several fast microbial processes rather than as a fixed temporal unit. Nevertheless, based on typical timescales of microbial responses to substrate inputs in soils, and by comparison with previous modeling and experimental studies (Wiesenbauer et

al., 2024) the simulated period of 200 iterations likely corresponds to a short-term decomposition or growth phase on the order of a few days (probably less than ~ 10 d), capturing an initial pulse of microbial growth and resource exploitation. This order of magnitude is broadly consistent with microbial doubling times reported for fast-growing bacteria such as *Escherichia coli*, which under favorable conditions divides approximately every 59 min (Gangwe Nana et al., 2018). Since cells in our model can reproduce at most once per iteration, 200 iterations would correspond to roughly 200 h, or approximately 8 days, in line with the estimate above. This mapping between iterations and real time nonetheless remains approximate and should be interpreted qualitatively rather than as a strict quantitative conversion. The primary objective of the model was to capture relative differences between scenarios rather than to reproduce an exact temporal scaling, and this distinction should be kept in mind when interpreting the simulated timeframe.

4.2.3 Microbial parameters and carbon use efficiency

In our framework, carbon use efficiency (CUE) is calculated as the ratio between carbon retained as microbial biomass and the total carbon assimilated, the latter encompassing the costs associated with growth, maintenance, and motility. Because maintenance and motility costs directly shape microbial CUE, these parameters were deliberately included in the sensitivity analysis, which confirmed their measurable influence on model outcomes. The parameter values used in the main simulations were first selected to ensure the emergence and persistence of viable microbial populations within the pore networks, and, beyond this constraint, to represent different ecological strategies inspired by the classical r/K framework. Our aim was not to identify a single, universally optimal parameter set, but rather to test whether r- or K-like strategies consistently performed better under specific pore-scale environmental conditions. As the sensitivity analysis shows, various parameter combinations can produce a broad range of CUE outcomes, and combinations not explored in the present study may prove better suited to other micro-environmental conditions or ecological contexts. The selected parameter sets should therefore be interpreted as representative ecological archetypes rather than as definitive physiological values. Our focus on r- and K-type strategies was primarily a methodological choice, as this dichotomy offers a well-established and tractable conceptual framework for investigating microbial trade-offs and spatial adaptation in structured soil environments.

Although few studies explicitly quantify the allocation of resources among these different expenditures, our parameterization yields microbial carbon use efficiency (CUE) values ranging from 0.28 to 0.78, which correspond to values reported in the literature (He et al., 2024; Jones et al., 2018; Schnecker et al., 2023). Note that the CUE values reported for oligotrophic communities (up to 0.72; Ma et al., 2023) exceed our estimates, which probably reflects the simplifications inherent to our approach.

4.2.4 Model simplifications

In natural systems, microbial carbon use efficiency is influenced not only by carbon availability, but also by nitrogen and other nutrients, which can constrain growth and alter carbon allocation patterns (Dor et al., 2026). In the present model, we consider a single resource type, interpreted as carbon, which is treated as a "complete" substrate assumed to fulfill all microbial requirements for growth and maintenance. This simplification allows us to isolate the effects of spatial structure, pore connectivity, and microbial traits on carbon processing efficiency, without introducing additional constraints related to nutrient limitation. We recognize that this represents a significant limitation of the current framework, as it does not explicitly account for nutrient stoichiometry or potential nitrogen limitation, both of which are known to affect microbial metabolism and CUE in soils (Cui et al., 2021; Hu et al., 2022). Extending the model to incorporate multiple nutrient pools nonetheless represents a natural and relevant next step. In particular, future versions of the model could introduce an explicit C : N stoichiometric constraint, in which resource quality and microbial uptake would depend on elemental composition, and in which stoichiometric imbalances could limit microbial growth and metabolism. If nitrogen were uniformly and readily available throughout the pore network, the results obtained here would likely remain broadly similar. In contrast, heterogeneous spatial distributions of carbon and nitrogen substrates could generate localized nitrogen limitations, which are known to reduce microbial CUE by increasing the respiratory carbon costs associated with nutrient acquisition and maintenance (Endress et al., 2024; Yuan et al., 2019). Such spatial mismatches between carbon and nitrogen availability could therefore amplify the spatial heterogeneity in microbial activity and CUE observed within a single simulation, and represent a promising direction for future refinements of the model.

Another important simplification of the current model is that of oxygen. In this version, we did not simulate oxygen diffusion or oxygen-dependent constraints on microbial metabolism, meaning that oxygen limitation arising from high microbial respiration rates or restricted gas diffusion in water-filled pores is not represented. In natural soils, however, oxygen availability is strongly controlled by pore structure and moisture conditions: larger, better-connected pores tend to be more aerated and therefore support higher aerobic microbial activity, whereas oxygen diffusion becomes increasingly restricted in smaller or water-saturated pores, which can limit microbial respiration and substrate utilization even when carbon resources are otherwise available (e.g., Kravchenko et al., 2020; Ceriotti et al., 2022). Because our simulations were intentionally focused on the role of pore-scale connectivity, water films, and substrate acces-

sibility, microbial activity in the model is not constrained by oxygen availability. This assumption may lead to an overestimation of resource utilization under highly water-saturated conditions compared to natural systems, where reduced gas diffusion would be expected to limit aerobic microbial activity in the most water-filled portions of the pore network. Incorporating oxygen diffusion and redox constraints therefore represents an important direction for future development of the model, particularly for improving its realism under high-moisture conditions.

As already described, in the present version of the model, necromass is directly returned to the pool of available resources, corresponding to a recycling rate of 100 %. This represents a simplification of the microbial carbon cycle in soils (Camenzind et al., 2023) and must be taken into account when interpreting the model results. Empirical studies indicate that the actual recycling efficiency of microbial biomass in soils is considerably lower: although microorganisms are able to feed on microbial necromass, recycling rates rarely exceed 12 % (Kästner et al., 2021), and microbial necromass can represent more than half of total soil organic carbon stocks (Liang et al., 2019). The use of a 100 % recycling rate in the model is therefore not intended to realistically represent the fate of microbial necromass, but rather reflects a deliberate structural simplification, allowing carbon to remain within the system and be continuously available for microbial uptake without introducing an additional, poorly constrained parameter. This simplification should be kept in mind when interpreting the absolute carbon dynamics produced by the model; however, it is expected to affect all microbial strategies similarly, since necromass return applies uniformly across cell types, whereas the relative differences between strategies are primarily driven by spatial access to resources and pore-scale constraints.

4.3 Influence of pore size and connectivity on microbial access to and microbial utilization of carbon

The model results suggest that the CUE of microorganisms is largely determined by the pore environment. It has already been shown that organic matter turnover varies across different soil pore sizes (Chenu et al., 2025; Li et al., 2024; Maestrali et al., 2026; Pfeiffer et al., 2001; Xia et al., 2022) because the microbes that dominate in these different pore sizes have strategies that are adapted to their microenvironment such as fluctuations in humidity (Ceriotti et al., 2022; Kravchenko et al., 2020), available space (Chenu et al., 2001; Gupta and Germida, 1988), nutrient availability (Bouckaert et al., 2013) and predation pressure (Erktan et al., 2020; Wright et al., 1995). This study suggests that the geometry of the pores themselves selects the microbes capable of colonising the environment. Indeed, when confined in micropores, organic matter is physically protected not only through exclusion by pore size, but also due to pore tortuosity, which modulates both substrate diffusion and microbial access. In our simulations, we observed that even when motile cells were close to small pores, their effective access to resources was limited by the tortuosity of the pore network. Although motile bacteria are capable of detecting chemical gradients, the establishment and continuity of these gradients depend on the connectivity of the pores and the continuity of the water film. In highly tortuous or poorly connected pore networks, chemical gradients can be weak, discontinuous, or spatially misleading, limiting the ability of motile cells to effectively reach nearby resource areas. For example, a flagellated bacterium may not effectively reach an organic matter particle located just a few micro-meters away if the accessible pathways are long or disconnected, whereas a non-motile bacterium already positioned nearby can exploit the resource via diffusion without incurring the energy cost of motility. These results are consistent with previous studies showing that tortuosity significantly influences bacterial mobility by increasing the complexity of the paths that bacteria must follow in porous media, thereby reducing their effective diffusion and transport rates. Using magnetic resonance imaging, it has been shown that the swimming behavior of bacteria such as *Pseudomonas putida* is strongly impeded by the pore structure (Olson et al., 2005). Bacterial motility patterns, particularly path lengths and turning angles, interact with surface adhesion in porous media, further increasing apparent tortuosity and affecting bacterial movement (Narayanaswamy et al., 2009). Experimental and modeling studies have demonstrated that smaller pores and more tortuous paths reduce the average free-swimming distances of bacteria, hindering their self-propulsion (Dehkharghani et al., 2023; Duffy et al., 1995).

This work suggests that the water regime (low water or water-saturated) modulates the influence of pore size on microbial communities. Under conditions with low water and organic matter in the macropores, motile cells achieve a higher CUE, suggesting that water creates connected pathways without completely restricting motility. This configuration allows motile cells to access resources while experiencing fewer diffusional constraints: resources diffuse only in the available water film and are therefore less "diluted" compared to a situation where pores are completely saturated with water. Our simulations suggest that r-strategist populations, characterized by their rapid growth, exploit this situation particularly well by efficiently colonizing accessible surfaces.

Water connectivity, rather than the nominal spatial distribution of resources, appears to be a key factor shaping resource accessibility at the pore scale, and this may help explain the effects of pore size reported above. Indeed, while the spatial distribution of organic resources remains identical across moisture treatments (Fig. 1), the volume of water accessible to a given cell, and therefore its access to dissolved substrates, differs substantially depending on the extent of water connectivity. Under low-water conditions, microbial cells and dissolved substrates are largely restricted to the re-

maining water films, so that resource diffusion, and hence the resupply of dissolved carbon, is limited to the connected volume of water film surrounding a given cell. Isolated, disconnected water pockets can still sustain local microbial activity as long as locally available resources persist, but they cannot receive further resource input from the rest of the pore network. This constraint affects motile and immobile strategists differently. Because active movement is itself limited to the same connected water film as diffusion, motile cells cannot bypass disconnected zones; however, within a connected volume, they can actively explore and relocate toward locally resource-rich areas rather than depending passively on diffusion to bring resources to them. Immobile cells, in contrast, remain confined to their initial location and depend entirely on the volume of water connected to that specific position for access to dissolved carbon. Consequently, immobile cells located in small or poorly connected water volumes under low-moisture conditions are more likely to become resource-limited, independently of the amount of resource nominally present in their vicinity. Under water-saturated conditions, by contrast, connected water volumes are maximized throughout the matrix, and the distinction between accessible and inaccessible resources becomes largely irrelevant, allowing both motile and immobile strategists more uniform access to substrates. Taken together, these considerations suggest that the differences in microbial dynamics and CUE observed between moisture treatments arise primarily from changes in the volume of connected water mediating resource accessibility, rather than from differences in the underlying spatial distribution of resources, and that this effect is expected to be particularly pronounced for immobile microbial types.

4.4 Microbial motility as a competitive advantage depending on soil pore architecture

The simulations suggest that motility does not confer a universal competitive advantage, but instead leads to different outcomes depending on pore-scale environmental conditions. In well-connected, carbon-rich environments, motile cells benefit from increased access to spatially distributed resources, resulting in higher growth and competitive success. In contrast, in poorly connected or resource-limited environments, the energetic costs associated with motility reduce carbon allocation to growth, leading to lower CUE compared to immobile strategies. This trade-off reflects the additional biosynthesis, repair, and operating costs associated with flagellar motility (Kempes et al., 2017), and is consistent with experimental observations showing reduced growth under carbon limitation when motility is constitutively expressed (Lisevich et al., 2025). Here, we show that pore-scale physical constraints modulate this trade-off, determining when motility enhances or limits microbial efficiency.

In fully saturated macropores, bacteria can exhibit efficient "run-and-tumble" movements with long ballistic trajectories (Zhang et al., 2024). In contrast, in micropores, physical confinement forces motile cells to adopt a less efficient "swim-and-stop" or "jump-and-trap" movement, significantly eroding the advantages of motility. Because motility itself carries an intrinsic energetic cost, this loss of efficiency in confined spaces translates into a lower resource return per unit of energy invested in movement. The chemotaxis machinery further amplifies these resource costs (substrate detection, flagellar or ciliary activity, etc.), compounding the energetic burden of motility in already unfavourable micropore environments and further reducing net CUE (van Albada et al., 2009; Hoffmann et al., 2017). In this context, the relationship between motility and carbon distribution is crucial. As this study demonstrates, motile bacteria have maximum CUE when organic matter is located in macropores, where chemotactic movement towards carbon gradients is optimal. When organic matter is confined to micropores, the motility advantage decreases significantly because bacteria cannot physically access these areas. In direct contrast, in our simulations, sessile bacteria dominate in micropores, maximising CUE by minimising motility-related costs (13 %–19 % of the cellular resource budget in our models) and redirecting resources towards stress tolerance and growth efficiency. Indeed, in low-connectivity environments, Jin and Sengupta (2024) observe that passive dispersal (expansion through growth, attachment to motile vectors) can surpass active motility in resource efficiency, explaining the good performance of immobile microbes when organic matter is confined to micropores. Thus, since the prevalence of bacterial flagellar motility is strongly associated with soil carbon accessibility (Ramoneda et al., 2024), cell motility should be particularly associated with a copiotrophic lifestyle, which explains the large populations observed in the case of motile r-strategists with resource distribution in the largest pores. Ultimately, the environmental dependencies observed (pore size, moisture) suggest that microbial communities are evolving towards motility patterns optimised for their specific environments. Microbial motility is not universally advantageous, but rather represents a finely tuned adaptation to the interaction between pore architecture, carbon heterogeneity and resource trade-offs, with cascading effects on the carbon cycle at the ecosystem scale. Furthermore, under favourable moisture conditions, active cell motility plays a key role in the early colonisation process: bacterial communities with cellular motility are pioneers and often the first to colonise new surfaces, followed by other bacteria with other functional traits (Wang et al., 2025), leading to the colonisation of new microenvironments in the soil.

Our results suggest that the distinction between motile and immobile microbial strategies remains relevant even when considering larger spatial scales, as the benefits of motility are highly context-dependent rather than universal. In our simulations, the effectiveness of motility depends strongly on pore connectivity, water-film continuity, tortuosity, and the energetic costs associated with movement, indicating that microbial access to resources cannot simply be reduced to an optimization process independent of microbial traits. Instead,

spatial structure determines when motility becomes advantageous relative to immobile strategies, and when it does not. At coarser spatial resolutions, however, it may not be necessary to explicitly simulate individual microbial movement: the pore-scale effects highlighted here could instead be represented indirectly through emergent parameters capturing substrate accessibility, spatial connectivity, diffusion limitation, or temporal delays in resource exploitation (i.e., a form of lag phase). Exploring how such emergent representations could substitute for an explicit motile/immobile distinction in larger-scale models represents a promising direction for future work, though it falls beyond the scope of the present study.

4.5 Influence of pore size on the selection of microbial strategies (r or K)

The simulations show that pore architecture fundamentally structures microbial ecological strategies. It is known that micropores constitute preferential niches for oligotrophic taxa (Acidobacteriales, Frankiales, Firmicutes) specialised in the processing of complex carbon compounds (Li et al., 2024). These organisms have specific morphological adaptations, reduced cell sizes and filamentous shapes, that maximise nutrient absorption under resource-limited conditions (Chen et al., 2022).

Our simulations indicate that the environment, and in particular pore architecture, can strongly modulate the influence of life cycle parameters on carbon use efficiency (CUE). While r and K strategies represent well-established ecological archetypes (Pianka, 1970; Li et al., 2024), the conditions under which they maximise CUE are not universal but depend heavily on pore size and cell motility. Using a spatially-explicit model, our study shows that in large pores, maintenance cost emerged as the dominant parameter, influencing CUE outcomes differently for motile and immobile cells (Fig. 5). In small pores, the reproduction threshold played a central role. These results indicate that the effect of each parameters cannot be dissociated from the environmental context: the same parameter can increase CUE under certain pore conditions, but cause it to be reduced under others. Similar results have been reported in microbial ecology, where the spatial heterogeneity of soil pores is recognised as a determining factor in microbial metabolic strategies (Nunan et al., 2020; Portell et al., 2018).

Carbon distribution in the soil pores network appears to be the main mechanistic link between pore size and the selection of microbial strategies. Chen et al. (2022) showed that carbon-rich rhizospheric soils favour copiotrophs, while poor environments select oligotrophs, which accentuates contrasts in resource availability between microsites. The microarchitecture of pores induces marked biogeochemical gradients over a few micrometres: Li et al. (2024) measured significant variations in oxygen, water film thickness and diffusion between pore classes, with macropores exhibiting more dynamic physicochemical conditions, while micropores maintain more stable but resource-poor environments. This trade-off between stability and availability is a fundamental axis for sorting ecological strategies, with r-strategists exploiting large, variable but rich pores, and K-strategists specialising in small, stable but limited pores. These spatio-temporal dynamics are also consistent with the phenomenon described by Zelenev et al. (2000) in the BACWAVE model, which simulated 'bacterial waves' generated by the movement of a nutrient pulse and translated into spatial waves of microbial growth and mortality along roots. Similarly, our model highlights a similar phenomenon where motile cells, particularly r-strategists, move along resource gradients formed on pore walls, producing wave-like dynamics of colonisation and consumption comparable to those observed empirically in the rhizosphere.

Overall, the sensitivity analyses (supplementary data) showed that microbial responses strongly depended on interactions between pore structure, moisture conditions and microbial traits. Importantly, no single parameter combination emerged as universally optimal across all simulated conditions. Instead, the results suggest that microbial performance arises from trade-offs between physiological traits in interaction with pore-scale environmental structures. These findings support the relevance of the selected parameter ranges while also indicating that the framework could be extended beyond the classical r/K dichotomy. We chose to focus specifically on r- and K-like strategies because they represent well-established ecological archetypes that provide a robust conceptual framework for exploring microbial trade-offs. Their widespread use in ecology makes them particularly suitable for investigating how different life-history strategies interact with pore-scale environmental heterogeneity.

Our cellular automaton succeeds in reproducing several well-documented mechanisms of soil microbial ecology, such as the trade-offs between r and K strategies, the different dynamics of motile and immobile cells, and the strong selective role of pore architecture on CUE. This convergence between model outputs and empirical knowledge highlights the potential of minimalistic, mechanistic approaches to capture emergent ecosystem patterns without requiring a high degree of parametrization. By making explicit the links between cellular traits, spatial constraints and carbon cycling, our framework provides a transparent test bed for exploring hypotheses that are difficult to address empirically at the microscale. Beyond confirming the relevance of r and K archetypes, our results pave the way for extending the model towards a broader trait-based framework, such as the Y-A-S triangle (Fig. S15) (Ho et al., 2013; Malik et al., 2020), in order to represent the continuum of microbial strategies observed in soils.

5 Conclusion

This study employed a spatially explicit model to investigate how soil pore architecture, resource distribution, moisture and the life cycle characteristics of microorganisms jointly regulate microbial dynamics and carbon use efficiency. The results suggest that the physical structure is an active factor in microbial functioning, influencing both resource access and the outcome of ecological trade-offs.

Our results suggest that pore size and connectivity exert a dominant control over microbial carbon use efficiency, often surpassing the influence of intrinsic physiological parameters. In particular, heterogeneity at the pore scale determines whether traits such as motility confer a competitive advantage or become energetically detrimental. The utility of motility emerges as a context-dependent, beneficial in well-connected, resource-rich environments but disadvantageous under high spatial constraints or limited resource accessibility. Similarly, the performances of r- and K-strategies are not fixed but dynamically modulated by the spatial distribution of carbon and the physical accessibility imposed by pore networks. Beyond confirming established ecological patterns, our model reveals that microbial functioning cannot be understood without explicitly accounting for the interaction between spatial structure and trait trade-offs.

Our model supports the use of minimalist yet mechanistic approaches as powerful tools for bridging the gap between pore-scale processes and the ecosystem-scale carbon cycle. However, several limitations must be acknowledged. The assumption of complete and instantaneous recycling of microbial biomass, as well as the simplified representation of microbial traits, likely leads to an overestimation of carbon turnover rates. Future developments should aim to incorporate more realistic representations of necromass dynamics, the effect of mineral surfaces, and a broader continuum of microbial strategies. By explicitly linking pore geometry and microbial ecology, this work offers a new conceptual framework for improving our understanding of the carbon cycle at the fine scale.

Code and data availability. The code has been released on GitHub and is available at https://github.com/Maelmstr/soil-cellular-automaton, it can also be found via https://doi.org/10.5281/zenodo.21336136 (Maelmstr., 2026). The data obtained during this study are available at https://doi.org/10.5281/zenodo.23335725 (Maestrali, 2026).

Supplement. The supplement related to this article is available online at https://doi.org/10.5194/soil-12-1079-2026-supplement.

Author contributions. MM: Conceptualisation, data curation, formal analysis, methodology, visualisation, writing; XR: Conceptualisation, methodology, validation, writing (review and editing); NN: Writing (review and editing), validation, supervision; HW: Conceptualisation, validation; SAS: Writing (review and editing), validation, supervision; ASR: data curation, formal analysis, visualisation.

Competing interests. The contact author has declared that none of the authors has any competing interests.

Disclaimer. Publisher's note: Copernicus Publications remains neutral with regard to jurisdictional claims made in the text, published maps, institutional affiliations, or any other geographical representation in this paper. The authors bear the ultimate responsibility for providing appropriate place names. Views expressed in the text are those of the authors and do not necessarily reflect the views of the publisher.

Special issue statement. This article is part of the special issue "Advances in dynamic soil modelling across scales". It is not associated with a conference.

Acknowledgements. We gratefully acknowledge the support by the Agence Nationale de la Recherche and the Deutsche Forschungsgemeinschaft.

Financial support. This research has been supported by the Agence Nationale de la Recherche (grant no. ANR-22-CE92-0039-01) and the Deutsche Forschungsgemeinschaft (DFG) as part of the SoilPACMAN Project (DFG project no. 505667051).

Review statement. This paper was edited by Holger Pagel and reviewed by Sara König and one anonymous referee.

References

Allison, S. D.: Cheaters, diffusion and nutrients constrain decomposition by microbial enzymes in spatially structured environments, Ecol. Lett., 8, 626–635, https://doi.org/10.1111/j.1461-0248.2005.00756.x, 2005.

Allison, S. D.: A trait-based approach for modelling microbial litter decomposition, Ecol. Lett., 15, 1058–1070, https://doi.org/10.1111/j.1461-0248.2012.01807.x, 2012.

Barton, J. W. and Ford, R. M.: Mathematical model for characterization of bacterial migration through sand cores, Biotechnol. Bioeng., 53, 487–496, https://doi.org/10.1002/(SICI)1097-0290(19970305)53:5<487::AID-BIT6>3.0.CO;2-D, 1997.

Baveye, P. C., Rangel, D., Jacobson, A. R., Laba, M., Darnault, C., Otten, W., Radulovich, R., and Camargo, F. A. O.: From Dust Bowl to Dust Bowl: Soils are Still Very Much a Frontier of Science, Soil Sci. Soc. Am. J., 75, 2037–2048, https://doi.org/10.2136/sssaj2011.0145, 2011.

Bongiorno, G., Bünemann, E. K., Oguejiofor, C. U., Meier, J., Gort, G., Comans, R., Mäder, P., Brussaard, L., and de Goede, R.: Sensitivity of labile carbon fractions to tillage and organic matter management and their potential as comprehensive soil quality indicators across pedoclimatic conditions in Europe, Ecol. Indic., 99, 38–50, https://doi.org/10.1016/j.ecolind.2018.12.008, 2019.

Bouckaert, L., Sleutel, S., Loo, D. V., Brabant, L., Cnudde, V., Hoorebeke, L. V., and Neve, S. D.: Carbon mineralisation and pore size classes in undisturbed soil cores, Soil Res., 51, 14–22, https://doi.org/10.1071/SR12116, 2013.

Bresenham, J. E.: Algorithm for computer control of a digital plotter, IBM Syst. J., 4, 25–30, https://doi.org/10.1147/sj.41.0025, 1965.

Camenzind, T., Mason-Jones, K., Mansour, I., Rillig, M. C., and Lehmann, J.: Formation of necromass-derived soil organic carbon determined by microbial death pathways, Nat. Geosci., 16, 115–122, https://doi.org/10.1038/s41561-022-01100-3, 2023.

Cellular Automata – The Moore neighbourhood: https://cell-auto.com/neighbourhood/moore/, last access: 10 October 2026.

Ceriotti, G., Borisov, S. M., Berg, J. S., and de Anna, P.: Morphology and Size of Bacterial Colonies Control Anoxic Microenvironment Formation in Porous Media, Environ. Sci. Technol., 56, 17471–17480, https://doi.org/10.1021/acs.est.2c05842, 2022.

Chang, W.-S., Li, X., and Halverson, L. J.: Influence of water limitation on endogenous oxidative stress and cell death within unsaturated Pseudomonas putida biofilms, Environ. Microbiol., 11, 1482–1492, https://doi.org/10.1111/j.1462-2920.2009.01876.x, 2009.

Chen, H., Jing, Q., Liu, X., Zhou, X., Fang, C., Li, B., Zhou, S., and Nie, M.: Microbial respiratory thermal adaptation is regulated by r-/K-strategy dominance, Ecol. Lett., 25, 2489–2499, https://doi.org/10.1111/ele.14106, 2022.

Chenu, C., Hassink, J., and Bloem, J.: Short-term changes in the spatial distribution of microorganisms in soil aggregates as affected by glucose addition, Biol. Fertil. Soils, 34, 349–356, https://doi.org/10.1007/s003740100419, 2001.

Chenu, C., Pouteau, V., and Nunan, N.: Pore scale microbial biogeography across different soil types, Soil Biol. Biochem., 209, 109896, https://doi.org/10.1016/j.soilbio.2025.109896, 2025.

Cui, Y., Moorhead, D. L., Guo, X., Peng, S., Wang, Y., Zhang, X., and Fang, L.: Stoichiometric models of microbial metabolic limitation in soil systems, Global Ecol. Biogeogr., 30, 2297–2311, https://doi.org/10.1111/geb.13378, 2021.

Darrah, P. R.: Models of the rhizosphere: I. Microbial population dynamics around a root releasing soluble and insoluble carbon, Plant Soil, 133, 187–199, https://doi.org/10.1007/BF00009191, 1991.

Dehkharghani, A., Waisbord, N., and Guasto, J. S.: Self-transport of swimming bacteria is impaired by porous microstructure, Commun. Phys., 6, 18, https://doi.org/10.1038/s42005-023-01136-w, 2023.

Dignac, M.-F., Derrien, D., Barré, P., Barot, S., Cécillon, L., Chenu, C., Chevallier, T., Freschet, G. T., Garnier, P., Guenet, B., Hedde, M., Klumpp, K., Lashermes, G., Maron, P.-A., Nunan, N., Roumet, C., and Basile-Doelsch, I.: Increasing soil carbon storage: mechanisms, effects of agricultural practices and proxies. A review, Agron. Sustain. Dev., 37, 14, https://doi.org/10.1007/s13593-017-0421-2, 2017.

Dor, M., Guber, A. K., Tiemann, L., Kuzyakov, Y., and Kravchenko, A. N.: Nitrogen availability decouples soil pore size-defined microhabitat control of microbial carbon use efficiency, Soil Biol. Biochem., 221, 110249, https://doi.org/10.1016/j.soilbio.2026.110249, 2026.

Duffy, K. J., Cummings, P. T., and Ford, R. M.: Random walk calculations for bacterial migration in porous media, Biophys. J., 68, 800–806, https://doi.org/10.1016/S0006-3495(95)80256-0, 1995.

Dusenbery, D. B.: Minimum size limit for useful locomotion by free-swimming microbes, P. Natl. Acad. Sci. USA, 94, 10949–10954, https://doi.org/10.1073/pnas.94.20.10949, 1997.

Endress, M.-G., Dehghani, F., Blagodatsky, S., Reitz, T., Schlüter, S., and Blagodatskaya, E.: Spatial substrate heterogeneity limits microbial growth as revealed by the joint experimental quantification and modeling of carbon and heat fluxes, Soil Biol. Biochem., 197, 109509, https://doi.org/10.1016/j.soilbio.2024.109509, 2024.

Erktan, A., Or, D., and Scheu, S.: The physical structure of soil: Determinant and consequence of trophic interactions, Soil Biol. Biochem., 148, 107876, https://doi.org/10.1016/j.soilbio.2020.107876, 2020.

Fierer, N., Bradford, M. A., and Jackson, R. B.: Toward an Ecological Classification of Soil Bacteria, Ecology, 88, 1354–1364, https://doi.org/10.1890/05-1839, 2007.

Franzluebbers, A. J., Hons, F. M., and Zuberer, D. A.: Seasonal changes in soil microbial biomass and mineralizable c and n in wheat management systems, Soil Biol. Biochem., 26, 1469–1475, https://doi.org/10.1016/0038-0717(94)90086-8, 1994.

Gangwe Nana, G. Y., Ripoll, C., Cabin-Flaman, A., Gibouin, D., Delaune, A., Janniere, L., Grancher, G., Chagny, G., Loutelier-Bourhis, C., Lentzen, E., Grysan, P., Audinot, J.-N., and Norris, V.: Division-Based, Growth Rate Diversity in Bacteria, Front. Microbiol., 9, 849, https://doi.org/10.3389/fmicb.2018.00849, 2018.

Gao, Y., Zhou, J., Lin, T., Li, Y., Zeng, Q., Chen, S., Xiong, D., Zhang, Q., Yang, Z., and Yang, Y.: The dominance of K-strategy microbes enhances the potential of soil carbon decomposition under long-term warming, Appl. Soil Ecol., 206, 105854, https://doi.org/10.1016/j.apsoil.2024.105854, 2025.

Gupta, V. V. S. R. and Germida, J. J.: Distribution of microbial biomass and its activity in different soil aggregate size classes as affected by cultivation, Soil Biol. Biochem., 20, 777–786, https://doi.org/10.1016/0038-0717(88)90082-X, 1988.

Haynes, R. J.: Labile Organic Matter Fractions as Central Components of the Quality of Agricultural Soils: An Overview, Adv. Agron., 85, 221–268, https://doi.org/10.1016/S0065-2113(04)85005-3, 2005.

He, L., Lipson, D. A., Mazza Rodrigues, J. L., Mayes, M., Björk, R. G., Glaser, B., Thornton, P., and Xu, X.: Dynamics of Fungal and Bacterial Biomass Carbon in Natural Ecosystems: Site-Level Applications of the CLM-Microbe Model, J. Adv. Model. Earth Syst., 13, e2020MS002283, https://doi.org/10.1029/2020MS002283, 2021.

He, X., Abs, E., Allison, S. D., Tao, F., Huang, Y., Manzoni, S., Abramoff, R., Bruni, E., Bowring, S. P. K., Chakrawal, A., Ciais, P., Elsgaard, L., Friedlingstein, P., Georgiou, K., Hugelius, G., Holm, L. B., Li, W., Luo, Y., Marmasse, G., Nunan, N., Qiu, C., Sitch, S., Wang, Y.-P., and Goll, D. S.: Emerging multiscale

insights on microbial carbon use efficiency in the land carbon cycle, Nat. Commun., 15, 8010, https://doi.org/10.1038/s41467-024-52160-5, 2024.

Ho, A., Kerckhof, F.-M., Luke, C., Reim, A., Krause, S., Boon, N., and Bodelier, P. L. E.: Conceptualizing functional traits and ecological characteristics of methane-oxidizing bacteria as life strategies, Environ. Microbiol. Rep., 5, 335–345, https://doi.org/10.1111/j.1758-2229.2012.00370.x, 2013.

Hoffmann, S., Schmidt, C., Walter, S., Bender, J. K., and Gerlach, R. G.: Scarless deletion of up to seven methyl-accepting chemotaxis genes with an optimized method highlights key function of CheM in Salmonella Typhimurium, PLOS ONE, 12, e0172630, https://doi.org/10.1371/journal.pone.0172630, 2017.

Hu, J., Huang, C., Zhou, S., and Kuzyakov, Y.: Nitrogen addition to soil affects microbial carbon use efficiency: Meta-analysis of similarities and differences in ^{13}C and ^{18}O approaches, Global Change Biol., 28, 4977–4988, https://doi.org/10.1111/gcb.16226, 2022.

Hudson, B. D.: Soil organic matter and available water capacity, J. Soil Water Conserv., 49, 189–194, https://doi.org/10.1080/00224561.1994.12456850, 1994.

Jenkinson, D. S. and Powlson, D. S.: The effects of biocidal treatments on metabolism in soil – V: A method for measuring soil biomass, Soil Biol. Biochem., 8, 209–213, https://doi.org/10.1016/0038-0717(76)90005-5, 1976.

Jin, C. and Sengupta, A.: Microbes in porous environments: from active interactions to emergent feedback, Biophys. Rev., 16, 173–188, https://doi.org/10.1007/s12551-024-01185-7, 2024.

Jones, D. L., Hill, P. W., Smith, A. R., Farrell, M., Ge, T., Banning, N. C., and Murphy, D. V.: Role of substrate supply on microbial carbon use efficiency and its role in interpreting soil microbial community-level physiological profiles (CLPP), Soil Biol. Biochem., 123, 1–6, https://doi.org/10.1016/j.soilbio.2018.04.014, 2018.

Kästner, M., Miltner, A., Thiele-Bruhn, S., and Liang, C.: Microbial Necromass in Soils – Linking Microbes to Soil Processes and Carbon Turnover, Front. Environ. Sci., 9, https://doi.org/10.3389/fenvs.2021.756378, 2021.

Kempes, C. P., van Bodegom, P. M., Wolpert, D., Libby, E., Amend, J., and Hoehler, T.: Drivers of Bacterial Maintenance and Minimal Energy Requirements, Front. Microbiol., 8, https://doi.org/10.3389/fmicb.2017.00031, 2017.

Kravchenko, A. N. and Guber, A. K.: Soil pores and their contributions to soil carbon processes, Geoderma, 287, 31–39, https://doi.org/10.1016/j.geoderma.2016.06.027, 2017.

Kravchenko, A. N., Guber, A. K., Razavi, B. S., Koestel, J., Quigley, M. Y., Robertson, G. P., and Kuzyakov, Y.: Reply to: Variables in the effect of land use on soil extrapore enzymatic activity and carbon stabilization by Glenn (2020), Nat. Commun., 11, 6427, https://doi.org/10.1038/s41467-020-19901-8, 2020.

Lehmann, J., Hansel, C., Kaiser, C., Kleber, M., Maher, K., Manzoni, S., Nunan, N., Reichstein, M., Schimel, J., and Torn, M.: Persistence of soil organic carbon caused by functional complexity, Nat. Geosci., 13, 1–6, 2020.

Li, Z., Kravchenko, A. N., Cupples, A., Guber, A. K., Kuzyakov, Y., Philip Robertson, G., and Blagodatskaya, E.: Composition and metabolism of microbial communities in soil pores, Nat. Commun., 15, 3578, https://doi.org/10.1038/s41467-024-47755-x, 2024.

Liang, C., Amelung, W., Lehmann, J., and Kästner, M.: Quantitative assessment of microbial necromass contribution to soil organic matter, Global Change Biol., 25, 3578–3590, https://doi.org/10.1111/gcb.14781, 2019.

Libohova, Z., Seybold, C., Wysocki, D., Wills, S., Schoeneberger, P., Williams, C., Lindbo, D., Stott, D., and Owens, P. R.: Reevaluating the effects of soil organic matter and other properties on available water-holding capacity using the National Cooperative Soil Survey Characterization Database, J. Soil Water Conserv., 73, 411–421, https://doi.org/10.2489/jswc.73.4.411, 2018.

Lisevich, I., Colin, R., Yang, H. Y., Ni, B., and Sourjik, V.: Physics of swimming and its fitness cost determine strategies of bacterial investment in flagellar motility, Nat. Commun., 16, 1731, https://doi.org/10.1038/s41467-025-56980-x, 2025.

Ma, S., Zhu, W., Wang, W., Li, X., and Sheng, Z.: Microbial assemblies with distinct trophic strategies drive changes in soil microbial carbon use efficiency along vegetation primary succession in a glacier retreat area of the southeastern Tibetan Plateau, Sci. Total Environ., 867, 161587, https://doi.org/10.1016/j.scitotenv.2023.161587, 2023.

Maelmstr.: Maelmstr/soil-cellular-automaton: Cellular automaton (Version v1.0.0), Zenodo [computer software], https://doi.org/10.5281/zenodo.21336136, 2026.

Maestrali, M.: Compiled data from CA simulations, Zenodo [data set], https://doi.org/10.5281/zenodo.23335725, 2026.

Maestrali, M., Raynaud, X., Wu, H., Schweizer, S. A., Guillot, I., Lerch, T., Paolillo, S., and Nunan, N.: How is the carbon use efficiency of microbial communities distributed within the soil pore network, Appl. Soil Ecol., 219, 106771, https://doi.org/10.1016/j.apsoil.2025.106771, 2026.

Malik, A. A., Martiny, J. B. H., Brodie, E. L., Martiny, A. C., Treseder, K. K., and Allison, S. D.: Defining trait-based microbial strategies with consequences for soil carbon cycling under climate change, ISME J., 14, 1–9, 2020.

McLauchlan, K. K. and Hobbie, S. E.: Comparison of Labile Soil Organic Matter Fractionation Techniques, Soil Sci. Soc. Am. J. 68, 1616–1625, https://doi.org/10.2136/sssaj2004.1616, 2004.

Narayanaswamy, K., Ford, R. M., Smith, J. A., and Fernandez, E. J.: Surface association of motile bacteria and apparent tortuosity values in packed column experiments, Water Resour. Res., 45, https://doi.org/10.1029/2008WR006851, 2009.

Newman, E. I. and Watson, A.: Microbial abundance in the rhizosphere: A computer model, Plant Soil, 48, 17–56, https://doi.org/10.1007/BF00015157, 1977.

Nunan, N., Schmidt, H., and Raynaud, X.: The ecology of heterogeneity: soil bacterial communities and C dynamics, Philos. Trans. R. Soc. B Biol. Sci., 375, 20190249, https://doi.org/10.1098/rstb.2019.0249, 2020.

Olson, M. S., Ford, R. M., Smith, J. A., and Fernandez, E. J.: Analysis of Column Tortuosity for $MnCl_2$ and Bacterial Diffusion Using Magnetic Resonance Imaging, Environ. Sci. Technol., 39, 149–154, https://doi.org/10.1021/es049577x, 2005.

Or, D., Smets, B. F., Wraith, J. M., Dechesne, A., and Friedman, S. P.: Physical constraints affecting bacterial habitats and activity in unsaturated porous media – a review, Adv. Water Resour., 30, 1505–1527, https://doi.org/10.1016/j.advwatres.2006.05.025, 2007.

Otten, W., Hall, D., Harris, K., Ritz, K., Young, I. M., and Gilligan, C. A.: Soil physics, fungal epidemiology and the

spread of Rhizoctonia solani, New Phytol., 151, 459–468, https://doi.org/10.1046/j.0028-646x.2001.00190.x, 2001.

Panikov, N. S.: Understanding and prediction of soil microbial community dynamics under global change, Appl. Soil Ecol., 11, 161–176, https://doi.org/10.1016/S0929-1393(98)00143-7, 1999.

Peng, J., Liu, H., Sun, Y., Liu, Q., Li, J., and Dong, Y.: Shift in soil bacterial communities from K- to r-strategists facilitates adaptation to grassland degradation, Land Degrad. Dev., 33, https://doi.org/10.1002/ldr.4304, 2022.

Pfeiffer, T., Schuster, S., and Bonhoeffer, S.: Cooperation and Competition in the Evolution of ATP-Producing Pathways, Science, 292, 504–507, https://doi.org/10.1126/science.1058079, 2001.

Pianka, E. R.: On r- and K-Selection, Am. Nat., 104, 592–597, https://doi.org/10.1086/282697, 1970.

Portell, X., Pot, V., Garnier, P., Otten, W., and Baveye, P. C.: Microscale Heterogeneity of the Spatial Distribution of Organic Matter Can Promote Bacterial Biodiversity in Soils: Insights From Computer Simulations, Front. Microbiol., 9, https://doi.org/10.3389/fmicb.2018.01583, 2018.

Pot, V., Portell, X., Otten, W., Garnier, P., Monga, O., and Baveye, P. C.: Accounting for soil architecture and microbial dynamics in microscale models: Current practices in soil science and the path ahead, Eur. J. Soil Sci., 73, e13142, https://doi.org/10.1111/ejss.13142, 2021.

R: The R Project for Statistical Computing, https://www.r-project.org/, last access: 29 October 2026.

Rabot, E., Wiesmeier, M., Schlüter, S., and Vogel, H.-J.: Soil structure as an indicator of soil functions: A review, Geoderma, 314, 122–137, 2018.

Ramoneda, J., Fan, K., Lucas, J. M., Chu, H., Bissett, A., Strickland, M. S., and Fierer, N.: Ecological relevance of flagellar motility in soil bacterial communities, ISME J., 18, wrae067, https://doi.org/10.1093/ismejo/wrae067, 2024.

Ray, N., Rupp, A., and Prechtel, A.: Discrete-continuum multiscale model for transport, biomass development and solid restructuring in porous media, Adv. Water Resour., 107, 393–404, https://doi.org/10.1016/j.advwatres.2017.04.001, 2017.

Reznick, D., Bryant, M., and Bashey, F.: r- and K-Selection Revisited: The Role of Population Regulation in Life-History Evolution, Ecology, 83, 1509–1520, https://doi.org/10.2307/3071970, 2002.

Ritschel, T. and Totsche, K. U.: Modeling the formation of soil microaggregates, Comput. Geosci., 127, 36–43, https://doi.org/10.1016/j.cageo.2019.02.010, 2019.

Rötzer, M., Braunmiller, H., Lehndorff, E., Ray, N., Scheibe, A., and Prechtel, A.: Coupled C and N turnover in a dynamic pore scale model reveal the impact of exudate quality on microbial necromass formation, SOIL, 12, 205–226, https://doi.org/10.5194/soil-12-205-2026, 2026.

Schimel, J. and Schaeffer, S. M.: Microbial control over carbon cycling in soil, Front. Microbiol., 3, https://doi.org/10.3389/fmicb.2012.00348, 2012.

Schlüter, S., Sammartino, S., and Koestel, J.: Exploring the relationship between soil structure and soil functions via pore-scale imaging, Geoderma, 370, 114370, https://doi.org/10.1016/j.geoderma.2020.114370, 2020.

Schlüter, S., Gil, E., Doniger, T., Applebaum, I., and Steinberger, Y.: Abundance and community composition of free-living nematodes as a function of soil structure under different vineyard managements, Appl. Soil Ecol., 170, 104291, https://doi.org/10.1016/j.apsoil.2021.104291, 2022.

Schnecker, J., Baldaszti, L., Gündler, P., Pleitner, M., Sandén, T., Simon, E., Spiegel, F., Spiegel, H., Urbina Malo, C., Zechmeister-Boltenstern, S., and Richter, A.: Seasonal dynamics of soil microbial growth, respiration, biomass, and carbon use efficiency in temperate soils, Geoderma, 440, 116693, https://doi.org/10.1016/j.geoderma.2023.116693, 2023.

Shi, A., Chakrawal, A., Manzoni, S., Fischer, B. M. C., Nunan, N., and Herrmann, A. M.: Substrate spatial heterogeneity reduces soil microbial activity, Soil Biol. Biochem., 152, 108068, https://doi.org/10.1016/j.soilbio.2020.108068, 2021.

Smet, S., Plougonven, E., Leonard, A., Degré, A., and Beckers, E.: X-ray Micro-CT: How Soil Pore Space Description Can Be Altered by Image Processing, Vadose Zone J., 17, 160049, https://doi.org/10.2136/vzj2016.06.0049, 2018.

Sparling, G. P. and West, A. W.: A direct extraction method to estimate soil microbial C: calibration in situ using microbial respiration and ^{14}C labelled cells, Soil Biol. Biochem., 20, 337–343, https://doi.org/10.1016/0038-0717(88)90014-4, 1988.

van Albada, S. B., Tănase-Nicola, S., and ten Wolde, P. R.: The switching dynamics of the bacterial flagellar motor, Molec. Syst. Biol., 5, 316, https://doi.org/10.1038/msb.2009.74, 2009.

Wang, G. and Or, D.: Aqueous films limit bacterial cell motility and colony expansion on partially saturated rough surfaces, Environ. Microbiol., 12, 1363–1373, https://doi.org/10.1111/j.1462-2920.2010.02180.x, 2010.

Wang, Y., Ebrahimi, A., Chen, G., Zhang, Z., Zhu, K., Franklin, S., Jin, Y., Liu, Y., and Wang, G.: Active motility and chemotactic movement regulate the microbial early-colonization and biodiversity, Geoderma, 460, 117419, https://doi.org/10.1016/j.geoderma.2025.117419, 2025.

Weller, U., Albrecht, L., Schlüter, S., and Vogel, H.-J.: An open Soil Structure Library based on X-ray CT data, SOIL, 8, 507–515, https://doi.org/10.5194/soil-8-507-2022, 2022.

Wiesenbauer, J., König, A., Gorka, S., Marchand, L., Nunan, N., Kitzler, B., Inselsbacher, E., and Kaiser, C.: A pulse of simulated root exudation alters the composition and temporal dynamics of microbial metabolites in its immediate vicinity, Soil Biol. Biochem., 189, 109259, https://doi.org/10.1016/j.soilbio.2023.109259, 2024.

Wolfram, S.: Cellular Automaton Fluids 1: Basic Theory, in: Lattice Gas Methods For Partial Differential Equations, CRC Press, 1990.

Wright, D. A., Killham, K., Glover, L. A., and Prosser, J. I.: Role of Pore Size Location in Determining Bacterial Activity during Predation by Protozoa in Soil, Appl. Environ. Microbiol., 61, 3537–3543, 1995.

Xia, Q., Zheng, N., Heitman, J. L., and Shi, W.: Soil pore size distribution shaped not only compositions but also networks of the soil microbial community, Appl. Soil Ecol., 170, 104273, https://doi.org/10.1016/j.apsoil.2021.104273, 2022.

Young, I. M. and Crawford, J. W.: Interactions and Self-Organization in the Soil-Microbe Complex, Science, 304, 1634–1637, https://doi.org/10.1126/science.1097394, 2004.

Yuan, X., Niu, D., Gherardi, L. A., Liu, Y., Wang, Y., Elser, J. J., and Fu, H.: Linkages of stoichiometric imbalances to soil microbial respiration with increasing nitrogen addition: Evidence from

a long-term grassland experiment, Soil Biol. Biochem., 138, 107580, https://doi.org/10.1016/j.soilbio.2019.107580, 2019.

Zech, S., Ritschel, T., Ray, N., Totsche, K. U., and Prechtel, A.: How water connectivity and substrate supply shape the turnover of organic matter – Insights from simulations at the scale of microaggregates, Geoderma, 405, 115394, https://doi.org/10.1016/j.geoderma.2021.115394, 2022.

Zelenev, V. V., van Bruggen, A. H. C., and Semenov, A. M.: "BACWAVE," a Spatial-Temporal Model for Traveling Waves of Bacterial Populations in Response to a Moving Carbon Source in Soil, Microb. Ecol., 40, 260–272, 2000.

Zhang, H., Wetherington, M. T., Ko, H., FitzGerald, C. E., and Nirody, J. A.: Bacterial motility patterns adapt smoothly in response to spatial confinement and disorder, bioRxiv, https://doi.org/10.1101/2024.09.29.615714, 2024.

Zhao, X., Tian, P., Sun, Z., Liu, S., Wang, Q., and Zeng, Z.: Rhizosphere effects on soil organic carbon processes in terrestrial ecosystems: A meta-analysis, Geoderma, 412, 115739, https://doi.org/10.1016/j.geoderma.2022.115739, 2022.

Zheng, W., Fan, X., Chen, H., Ye, M., Yin, C., Wu, C., and Liang, Y.: The response patterns of r- and K-strategist bacteria to long-term organic and inorganic fertilization regimes within the microbial food web are closely linked to rice production, Sci. Total Environ., 942, 173681, https://doi.org/10.1016/j.scitotenv.2024.173681, 2024.